ACS APPLIED MATERIALS & INTERFACES

Research Article

Cite This: ACS Appl. Mater. Interfaces 2019, 11, 11262−11269

www.acsami.org

Microcompartments for Protection and Isolation of Nanoscale DNA Computing Elements

Aurora Fabry-Wood,[†] Madalyn Elise Fetrow,[†] Ayomide Oloyede,[†] Kyung-Ae Yang,[‖] Milan N. Stojanovic,[‖,⊥] Darko Stefanovic,[†,§] Steven W. Graves,*[,†,‡] Nick J. Carroll,*[,†,‡] and Matthew R. Lakin*[,†,§]

[†]Center for Biomedical Engineering, [‡]Department of Chemical and Biological Engineering, and [§]Department of Computer Science, University of New Mexico, Albuquerque, New Mexico 87131, United States

[‖]Division of Experimental Therapeutics, Department of Medicine, and [⊥]Departments of Biomedical Engineering and Systems Biology, Columbia University Medical Center, New York, New York 10032, United States

Supporting Information

ABSTRACT: Physical isolation of molecular computing elements holds the potential for increasing system complexity by enabling the reuse of standardized components and by protecting the components from environmental degradation. However, once elements have been compartmentalized, methods for communicating into these compartments are needed. We report the compartmentalization of steroid-responsive DNA aptamers within giant unilamellar vesicles (GUVs) that are permeable to steroid inputs. Monodisperse GUVs are loaded with aptamers using a microfluidic platform. We demonstrate the target-specific activation of individual aptamers within the GUVs and then load two noninterfering aptamers into the same GUV and demonstrate specific responses to all possible combinations of the two input steroids. Crucially, GUVs prevent the degradation of DNA components by nucleases, providing a potential mechanism for deploying nucleic acid components in vivo. Importantly, our compartments also prevent nonspecific cross-talk between complementary strands, thereby providing a method for parallel execution of cross-reacting molecular logic components. Thus, we provide a mechanism for spatially organizing molecular computing elements, which will increase system modularity by allowing standardized components to be reused.

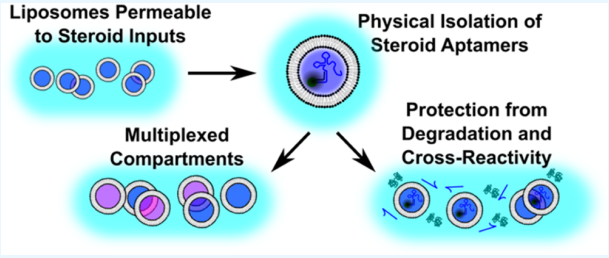

KEYWORDS: *biosensors, aptamers, steroids, giant unilamellar vesicles, microfluidics, compartmentalization, DNA computing*

INTRODUCTION

Molecular computation uses logic gates, built using biological polymers, to make decisions using nanoscale molecular constructs. Molecular computing is a particular instance of unconventional computing,[1] a field which seeks to implement computational behavior using a variety of nonstandard technologies. DNA, which is characterized by highly predictable thermodynamic and mechanical properties, is an ideal building block for designing these dynamic molecular systems, as Watson−Crick base pairing enables design of molecular interactions with high fidelity. However, most reported DNA-based systems operate in homogeneous, solution-phase systems, which lack spatial organization.[2−6] A key challenge when designing molecular circuits is nonspecific activation of circuit components, which occurs when output signals are generated in the absence of the designed activating stimulus, leading to lower signal-to-noise ratios. Nonspecific activation (also known as leakage) is particularly problematic in homogeneous, solution-phase DNA systems because any component could interact with any other component at any time. Mechanisms to limit nonspecific activation include meticulous sequence design, thresholding to suppress low-level leak signals,[7] incorporation of base mismatches to prevent formation of undesirable complexes,[8,9] structural designs that protect sequences vulnerable to leakage,[5,6] and domain-level motifs that mitigate leakage by increasing the number of spurious events required for leakage to occur.[10] Efforts to decrease leakage by restricting computing elements to DNA origami scaffolds[11−15] have also been made. Despite these elegant technical advancements, reducing nonspecific activation remains difficult for synthetic molecular computing systems. Our compartmentalized system eliminates nonspecific activation by physically isolating computing elements.

Living systems comprise highly organized sets of compartments, and these ensembles are directly tied to survival and reproduction. Each compartment contains specialized molecular circuitry, and communication between compartments is essential. From organelles to cells to tissues to organisms, the

Received: February 19, 2019
Accepted: March 8, 2019
Published: March 8, 2019

DOI: 10.1021/acsami.9b03143
ACS Appl. Mater. Interfaces 2019, 11, 11262−11269

flow of information is precisely controlled, and correct function relies on the spatial organization of biomolecular circuits that would otherwise interact in promiscuous, less-specific ways.[16] Lipid bilayers form the majority of compartments in cellular systems, including the cell membrane, nuclear envelope, and mitochondrial membranes. Here, we follow this biological example by physically isolating DNA-based molecular sensors from potentially deleterious interactions, in selectively permeable, membrane-bound compartments. Specifically, our model system uses giant unilamellar vesicles (GUVs). GUVs are compartments, with diameter ranging from 1 to 200 μm, bounded by a lipid bilayer with an aqueous center.[17] Our hypothesis is that preventing direct physical interaction between sensor elements and the external chemical environment can reduce (i) nonspecific sensor activation, (ii) cross-talk with other circuit elements, and (iii) environmental degradation. This study tests each aspect of the above hypothesis.

For a physically isolated molecular sensor to be useful, it must be capable of sensing the external chemical environment. In biological systems, signal transduction is achieved via integral membrane proteins or via passive diffusion (i.e., permeation of small nonpolar or moderately polar molecules directly across the cell membrane). Here, we demonstrate the latter approach by using steroids as a model stimulus capable of passively diffusing across a lipid bilayer. We recently reported a set of single-stranded DNA aptamers that specifically bind steroid targets and can be monitored with fluorescent microscopy.[18] These aptamers are ideal for the development of DNA-based biosensors isolated within lipid bilayers because steroids provide a method for signaling across the bilayer without disrupting it, which would directly expose the contents of the lipid bilayer to the external chemical environment.

Protecting sensors from the chemical environment is important because the human immune system has many defense mechanisms, such as nucleases that degrade foreign nucleic acids. A key goal of DNA nanotechnology is to deploy engineered systems in vivo for autonomous diagnostic, and potentially therapeutic, applications,[19] for which they must be stable in the presence of nucleases.[20−22] Our solution to this problem is to physically isolate the computing elements from nucleases that would otherwise degrade them, thereby preventing those nucleases from encountering and degrading the engineered nucleic acid components. Thus, our GUV system offers a model, which could also be applied to nanoscale vesicles, to deploy nucleic acid-based biosensors in an intracellular environment for extended periods of time. Finally, isolation of computing elements offers a route to implement more sophisticated behaviors by enabling the use of standardized components through physical isolation of functionally distinct but potentially cross-reacting components from each other.

RESULTS AND DISCUSSION

Microfluidics To Generate Monodisperse GUVs. We used a glass capillary microfluidic platform[17] to generate monodisperse GUVs, loaded with a range of aptamer cargos. Various aptamer cargos could easily be loaded because this system allows all phases [inner aqueous (IA), continuous, and oil] to be modulated independently (Figure 1A). In addition, this system requires the use of a polymer, poly(vinyl alcohol) (PVA) in this case, to increase the viscosity and stabilize the

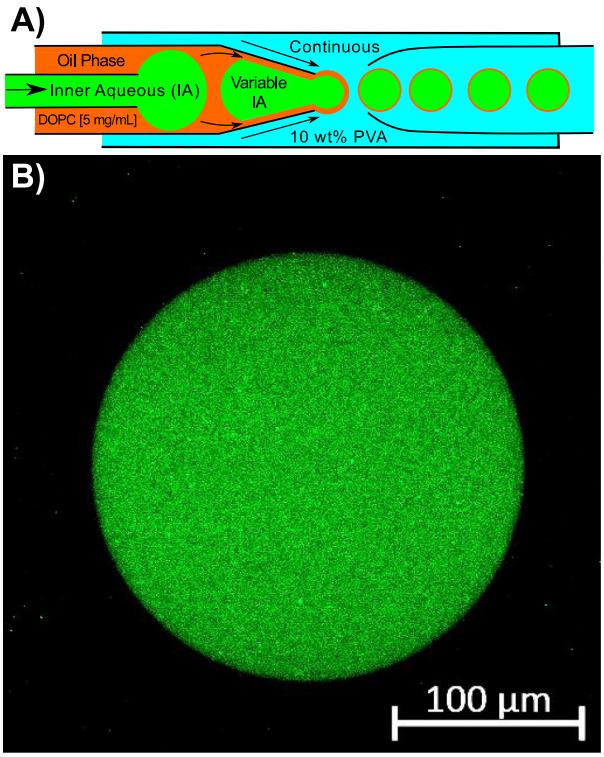

Figure 1. Microfluidic system. (A) For the initial experiments, GUVs were loaded with an IA phase of 10 wt % PVA in PBS, pH of 7.4, and a fluorescently tagged oligonucleotide (500 nM), to confirm microfluidic chip function and membrane stability in the presence of these compounds. The continuous phase consisted of 10 wt % PVA in PBS, pH 7.4, and the oil phase consisted of DOPC (5 mg/mL) in 36 vol % chloroform and 64 vol % hexane. See Movie S1 for imaged device operation. (B) Representative GUV imaged on a Zeiss LSM 800 Airyscan confocal microscope (488/520 nm). Scale bar: 100 μm.

lipid headgroups. Injection pumps are used for each of the phases, allowing flow rates to be modulated independently. Generally speaking, the continuous phase is run at the highest flow rate. This introduces shear forces that pinch the lipid stream, thereby forming vesicles. The rates of the IA and oil phases affect the shell thickness, which must be <500 nm to achieve stable GUVs.[23] Directly after fabrication, the GUVs are incubated in a collection solution, at which point a good solvent (chloroform in this case) moves into the solution, leaving behind a bad solvent (hexanes in this case), which gradually dewets, allowing the lipids to assemble into a bilayer with an expected thickness of 5 nm. If this dewetting process happens too quickly, the lipids will not organize into bilayers and the GUVs will burst. Saturating the collection solution with the good solvent helps to slow the dewetting process. The collection container is also essential for stability, as any hydrophobic surface will disrupt the GUVs, and therefore, we exclusively used glass containers for collection.

The initial experiments confirmed stability with the addition of salts and a buffer to the aqueous components, as the previously reported glass capillary system consisted of PVA (MW 13 000−23 000) in water. Nucleic acids require salt for hybridization, and we wanted to maintain a physiologically relevant pH; thus, phosphate-buffered saline (PBS) was selected and PVA was dissolved into the PBS at 10 wt %. This solution was used for both the IA phase and the

DOI: 10.1021/acsami.9b03143
ACS Appl. Mater. Interfaces 2019, 11, 11262−11269

continuous phase (Figure 1A; Movie S1 shows the device in operation). We also introduced a fluorescein (FAM)-labeled oligonucleotide (500 nM) into the IA phase and generated GUVs that were imaged on a Zeiss LSM 800 confocal microscope (Figure 1B). Having confirmed the GUV stability, various components could be loaded into the GUVs that were collected in a solution containing 5 wt % PVA in PBS. The higher PVA percentage within the GUVs caused them to settle in this solution, which was saturated with chloroform to slow the dewetting process, as described above.

DOGS.2 and CSS.1 Aptamer/Quenchers. Two previously reported aptamer−ligand pairs were selected: the DOGS.2 aptamer that binds deoxycorticosterone (DC) with high selectivity and the CSS.1 aptamer that binds cortisol (CS).[18] The published solubility for the DC steroid is 100 μg/mL (302.6 μM) in ethanol; however, solubility at 500 μM in an aqueous buffer was achieved. The two aptamers were labeled with spectrally distinct fluorophores: DOGS.2 with FAM and CSS.1 with ATTO647. Each aptamer was hybridized to a partially complementary quencher strand labeled with an Iowa Black quencher specific to the fluorophore, forming an aptamer/quencher (A/Q) pair (Figure 2). Proximity quenching between the fluorophore and the Iowa Black quencher results in low fluorescence in the absence of target. Binding of the corresponding steroid target causes the aptamer strand to change conformation, which displaces the quencher strand. The quencher is no longer in close proximity to the fluorophore and hence fluorescence increases. Neither aptamer is activated by the other, off-target ligand. We redesigned the stem region of the published sequences (which is not part of the conserved target binding aptamer sequence) so that the two A/Q pairs would not cross-react when placed in the same GUV.

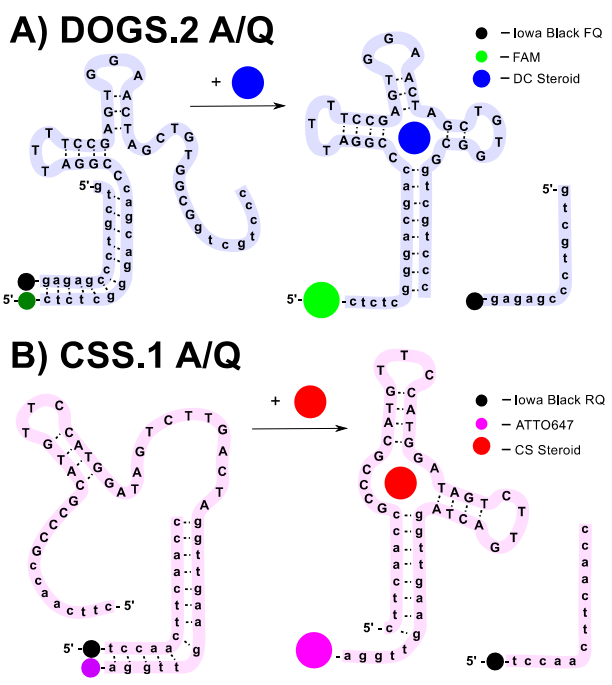

Figure 2. Aptamer structure and response to steroid inputs. (A) DOGS.2 aptamer is labeled with FAM and has a complementary quencher strand labeled with an Iowa Black FQ quencher. This A/Q pair is activated by the DC steroid, which causes a conformational change, ultimately displacing the quencher strand, resulting in an increase in FAM fluorescence. The uppercase bases represent the conserved target binding region of the aptamer strand, whereas the lowercase bases represent the stem region of the aptamer strand and the complementary quencher strand. (B) CSS.1 aptamer is labeled with ATTO647 and has a complementary strand labeled with the Iowa Black RQ quencher. This A/Q pair is activated by the CS steroid.

Responses of A/Q Pairs Isolated within GUVs. Aptamer function in 10 wt % PVA was first tested in a homogenous solution (see Materials and Methods and Supporting Information Figures S3 and S4 for details). Having fully characterized the behaviors of both the DOGS.2 and the CSS.1 aptamers in the PVA solution, each A/Q pair was loaded into GUVs individually using our microfluidic platform. The loaded GUVs were incubated at room temperature for an hour, to allow dewetting of the oil-phase solvents, at which point each steroid was added to a separate well containing ∼100 GUVs loaded with one of the A/Q pairs and incubated at room temperature for 1 h. Figure 3A shows confocal imagery of a GUV loaded with the DOGS.2 A/Q pair in the absence of steroid. Figure 3B is a GUV after 1 h of exposure to the nonspecific CS steroid (500 μM), and Figure 3C is a GUV 1 h after exposure to the target DC steroid (500 μM). We observe specific activation of the DOGS.2 A/Q pair by the DC steroid. During image processing, the grayscales were standardized across all samples. Figure 3D−F shows the same for the CSS.1 A/Q pair and we similarly observe specific aptamer activation by the CS steroid. However, the slower activation of the CSS.1 A/Q pair required an incubation period of 3 h. As the binding kinetics between both aptamer−target pairs are comparably fast in solution, we believe the slower activation here (1 h for the DC steroid and 3 h for the CS steroid) may be related to lower permeability of the CS steroid across the 1,2-dioleyl-*sn*-glycero-3-phosphocholine (DOPC) lipid bilayer. We believe that a proxy for this permeability may be found in the solubility of the DC and CS steroids. Literature values[24] for the solubility of DC and CS in water at 25 °C are 0.4 and 0.8 mM, respectively. Thus, we hypothesize that, because CS is more soluble, it is less likely to leave the outer aqueous phase in order to traverse the membrane, and therefore, the transmembrane diffusion rate (and hence the aptamer activation rate) would be slower for CS, and this hypothesis is supported by our experimental data. Here, we are making the assumption that transmembrane diffusion is the rate-limiting step in the aptamer activation process. Figure 4 shows the results of a quantitative analysis of the intensity for five replicate GUVs from the experiment shown and described in Figure 3. These results confirm the permeability of the steroid targets across the lipid bilayer and demonstrate signal transduction and specific detection in physically isolated membrane compartments.

We next tested the behavior with both the DOGS.2 and CSS.1 A/Q pairs in the same solution. Figure 5A shows fluorimetry data for the response of each aptamer in a homogeneous solution in the presence of the DC steroid, the CS steroid, and a combination of the DC and CS steroids. Having confirmed the function and specificity of the aptamers together in solution, we loaded both A/Q pairs into the same GUV. Figure 5B shows the quantification of five replicate GUVs after 3 h of exposure to individual or a combination of both steroids, and an example image of each is shown in Figure 5C−F. As seen in solution, these data show that our aptamer−

DOI: 10.1021/acsami.9b03143
ACS Appl. Mater. Interfaces 2019, 11, 11262−11269

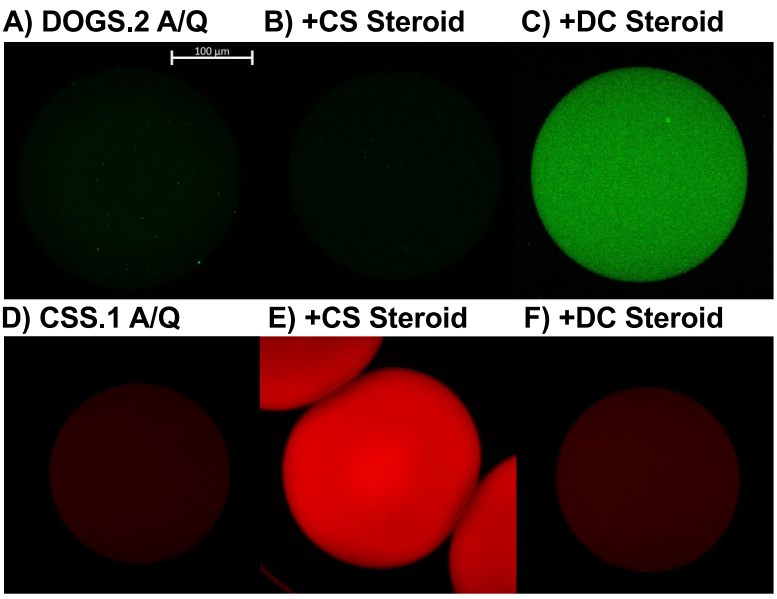

Figure 3. GUV response in the presence of various steroid inputs. (A) DOGS.2 aptamer (500 nM)/quencher (550 nM) in the absence of input. (B) DOGS.2 A/Q 1 h after the addition of the nonspecific CS steroid (500 μM). (C) DOGS.2 A/Q 1 h after the addition of the specific DC steroid (500 μM). (D) CSS.1 aptamer (500 nM)/quencher (550 nM) in the absence of input. (E) CSS.1 A/Q 3 h after the addition of the specific CS steroid (500 μM). (F) CSS.1 A/Q 3 h after the addition of the nonspecific DC steroid (500 μM). Scale bar: 100 μm.

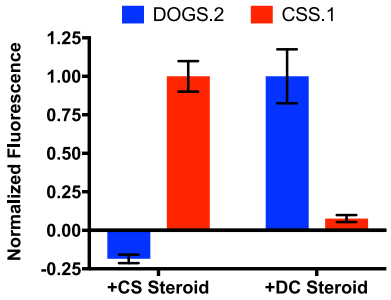

Figure 4. Aptamer activation in GUVs, with error analysis. Five GUVs were imaged for each of the reaction conditions presented in Figure 3 (error bars are 95% CI). The time points are as described in Figure 3, images were taken 1 h after DC was introduced and 3 h after CS was introduced. The FAM channel (488/520 nm) and ATTO647 channel (647/662 nm) values were calculated using a region of interest that was identical for all replicates. The plots were normalized to the mean of the A/Q pair as 0 and the mean of the target response as 1. Raw data are presented in Supporting Information Figure S5.

ligand sets are noninterfering. Furthermore, activation within the GUV is comparable to the experiments with individual A/Q pairs.

To demonstrate multiplexing, we created a solution with multiple populations of GUVs. Each GUV was loaded with either the DOGS.2 A/Q pair or the CSS.1 A/Q pair. Figure 6A shows the two populations in solution, in the absence of steroid targets. Even though the aptamers are quenched, it is still possible to determine which GUVs contain the FAM-labeled DOGS.2 A/Q pair and which contain the ATTO647-labeled CSS.2 A/Q pair. In Figure 6B, with the CS steroid (500 μM) added, we only see increased fluorescence in the GUVs loaded with CSS.1, whereas, in Figure 6C, with the addition of the DC steroid (500 μM), only the GUVs loaded with DOGS.2 brighten. Finally, in Figure 6D, with the addition of both the CS and the DC steroid targets, the fluorescence for all GUVs increases. Figure 6E shows the quantification of four replicate GUVs for each sample, further confirming the specificity of our aptamer–ligand sets in the context of multiplexed GUV populations. For this experiment, we used noninterfering sequences; however, the same experiment would work if multiple aptamers, with complementary regions that would cross-react in a homogeneous solution,[18] were loaded into separate GUVs in a single-tube assay. Although others have used lipid bilayers for compartmentalization of DNA-based molecular computing elements,[25−27] our microfluidic system provides a simple means of creating many compartments and does not require pores for signal transduction,[28] thereby maintaining a physical separation between the internal and external solutions.

Protection from Nucleases. To function in a biological environment, nucleic acid-based molecular computing systems must be protected from degradation by nucleases. If a nuclease can access an A/Q pair, it will completely degrade the individual strands, and the fluorophore and quencher will no longer be held in close proximity, resulting in an increase in fluorescence (Figure 7A). To test this hypothesis, we added DNAse I to the DOGS.2 A/Q pair in the 10 wt % PVA solution. DNAse I requires magnesium ions, and so we added Mg^{2+} (5 mM) to the solution. Figure 7B shows the anticipated increase in fluorescence in the presence of functional DNAse I, which is equivalent to that caused by the addition of the DC steroid target. To confirm that this was due to degradation by the DNAse and not some other mechanism (e.g., aptamer binding to the nuclease protein itself), we exposed the A/Q pair to denatured DNAse (20 min at 95 °C) and observed only negligible increase in the fluorescent signal.

To demonstrate the ability of GUVs to protect DNA components from nucleases (Figure 7C), we loaded GUVs with the DOGS.2 A/Q pair, including Mg^{2+} (5 mM) in all aqueous solutions (the IA, continuous, and collection solutions) for this experiment. We then added denatured

DOI: 10.1021/acsami.9b03143
ACS Appl. Mater. Interfaces 2019, 11, 11262−11269

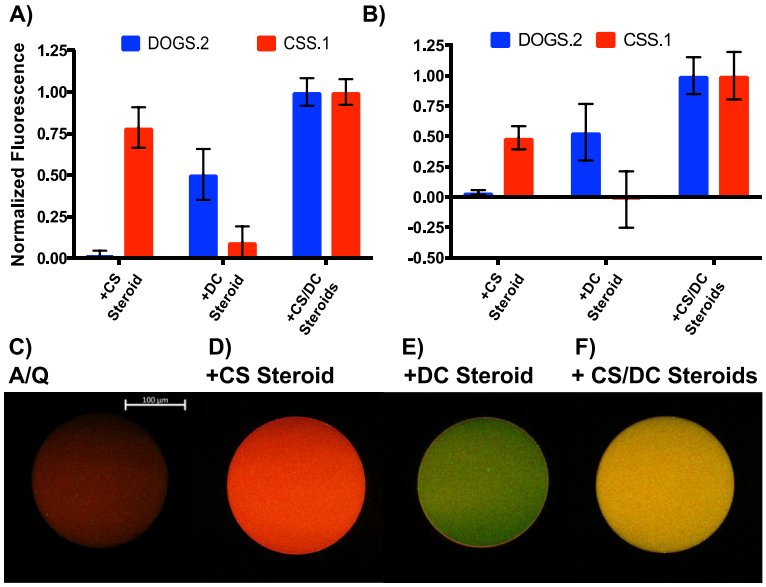

Figure 5. Responses of both aptamers within a single GUV. (A) Fluorimetry experiment with both DOGS.2 and CSS.1 A/Q present. Both aptamer strands are at 50 nM, and both quenchers are at 55 nM. Both steroids were added at 150 μM, with a total steroid concentration of 300 μM for the +DC/CS steroid samples. (B) Fluorescent microscopy analysis, with both DOGS.2 and CSS.1 in the same GUV, in the presence of DC and CS steroids, and a combination of both steroid inputs. (C) Composite image of both the FAM (488/520 nm) and the ATTO 647 (647/662 nm) channels in the absence of inputs. (D) Same as C with the CS steroid (500 μM). (E) Same as C with the DC steroid (500 μM). (F) Same as C, with both steroids each at 500 μM, for a total steroid concentration of 1 mM. Scale bar: 100 μm.

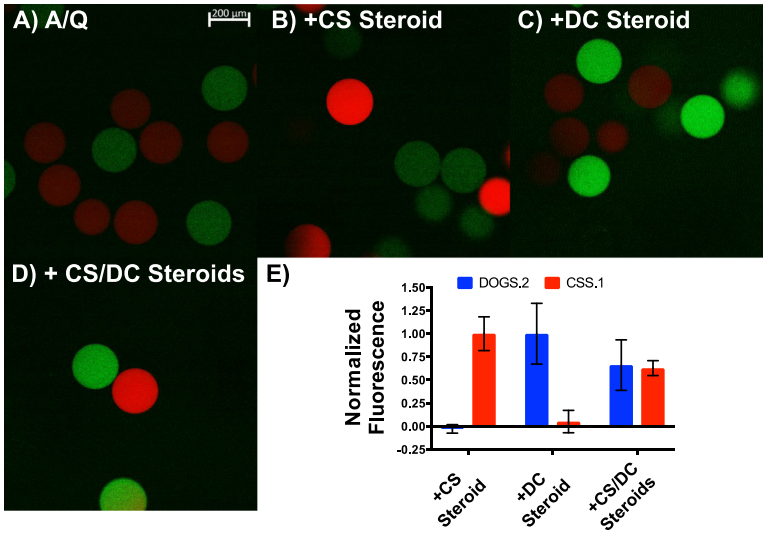

Figure 6. Multiplexing GUV compartments. (A) Two populations of GUVs loaded with individual aptamers, in the same solution. (B) Same as A, in the presence of CS steroid (500 μM). (C) Same as A, in the presence of DC steroid (500 μM). (D) Same as A, in the presence of both CS and DC steroids. (E) Analysis of four replicates, error bars represent 95% CI, on the FAM (488/520 nm, DOGS.2) and ATTO647 (647/662 nm, CSS.1) channels. Scale bar: 200 μm.

DNAse I, functional DNAse I, functional DNAse I, and the DC steroid target and as an absolute positive control the DC steroid target on its own to GUV solutions (Figure 7D). We saw full protection from DNAse I when our A/Q pair was isolated in a GUV; the response was equivalent to the denatured DNAse I sample, indicating full protection. We interpret this as the GUV membrane providing a physical barrier that prevents the DNAse from reaching the A/Q inside. To confirm DC steroid activation of DOGS.2 in the presence of the fully functional DNAse, we exposed the GUVs to both the DNAse and the DC steroid for 1 h and saw an increase in fluorescence. However, the increase in fluorescence for DC on its own was stronger and more consistent, possibly because of sequestration of the steroid by the DNAse.

Protection from Complementary Strands. Another key advantage of physically isolating molecular circuits is that nucleotide sequences can be reused in different parts of the circuit without cross-talk.[13] To demonstrate that GUVs can protect internal components from undesired activation by partially complementary sequences, we introduced a strand

DOI: 10.1021/acsami.9b03143
ACS Appl. Mater. Interfaces 2019, 11, 11262−11269

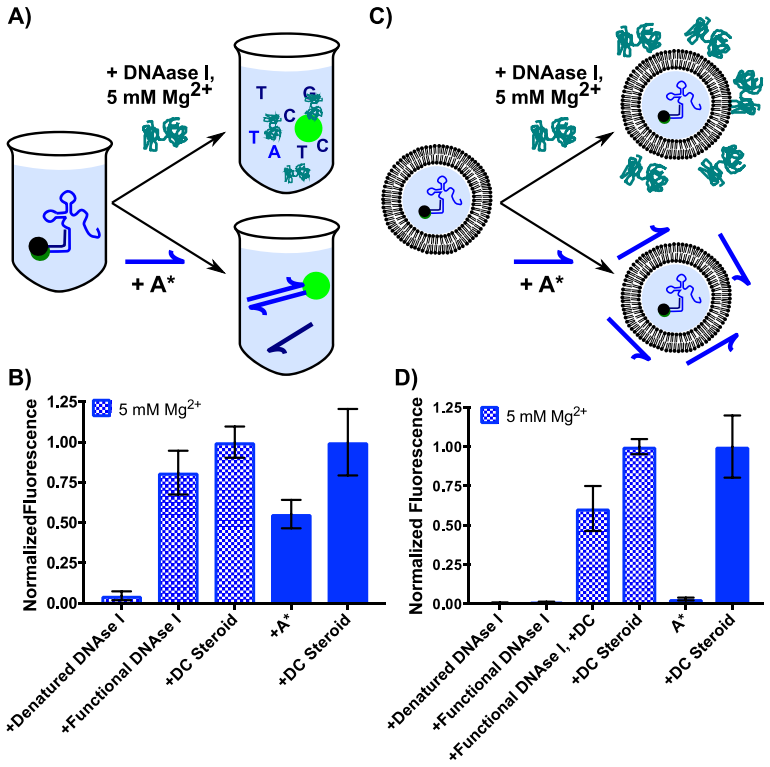

Figure 7. Protection from nucleases and complementary strands. (A) Schematic illustrating solution-phase experiments, with either the addition of DNAse I or a strand that is fully complementary to the DOGS.2 aptamer (A*). In this case, all reactants are free to interact—DNAse I will degrade nucleic acids and complementary strands will form duplexes. (B) Fluorimetry experiment with the DOGS.2 aptamer (100 nM)/quencher (110 nM) in the presence of denatured DNAse I (10 μM), functional DNAse I (10 μM), the DC steroid target (500 μM), in the presence of Mg^{2+}. On the same bar chart, we have DOGS.2 aptamer (500 nM)/quencher (550 nM) in the presence of A* (600 nM), and the DC steroid target (500 μM) in the absence of Mg^{2+}. (C) Schematic illustrating GUV experiments, where the lipid bilayer prevents both DNAse I and A* from interacting with the DOGS.2 A/Q pair. As illustrated in both A and C, the DNAse I experiments require 5 mM Mg^{2+}, which was added into all phases for the GUV experiment. The A* experiments do not have Mg^{2+}. Error bars represent 95% CI for five replicates. (D) GUV experiment, with the DOGS.2 aptamer (500 nM)/quencher (550 nM) loaded into a GUV with 5 mM Mg^{2+} in all phases. The same denatured DNAse was added as a second negative control. For this experiment, we added functional DNAse in the presence of the DC steroid target (500 μM). As a true positive control, the DC steroid target was added at 500 μM. Error bars represent 95% CI for five replicates.

(A*) that is fully complementary to the DOGS.2 aptamer strand. Our hypothesis was that the A* strand would interact with the A/Q pair when in bulk solution (Figure 7A) but would be prevented from doing so by a GUV membrane (Figure 7C). Our fluorimetry experiment, in a homogeneous solution, studying the interactions of the DOGS.2 aptamer (500 nM)/quencher (550 nM) with the complementary A* strand (600 nM) (Figure 7B) shows activation of the fluorescent response, albeit slower and weaker than for the DC steroid input. This could be due to a kinetic trap that prevents the formation of the A/A* complex, which is predicted to be the most thermodynamically stable conformation owing to complete complementarity and a net increase in the number of base pairs. An alternative explanation, however, could be proximal base quenching of the fluorophore on the aptamer strand, as has previously been reported by Padirac et al.[29] We demonstrated protection of the aptamers against the complementary strand by loading GUVs with the DOGS.2 A/Q and exposed them to an external solution containing A* (Figure 7D). The lack of response when A* is present in the external solution confirms protection of the A/Q pair from A* strand by the GUV and indicates that standardized strands (which in bulk solution would cross-react due to sequence complementarity) can be used in a solution that has been compartmentalized using our system.

CONCLUSIONS

Using a previously reported microfluidic platform, DNA aptamers were isolated within GUVs. Initially, individual aptamers were isolated within GUVs. We then isolated two aptamers within the same GUV and finally we monitored behaviors with a mixture of two GUV populations, each with a single A/Q pair, within the same solution. These aptamer-based molecular computing elements were activated by steroid inputs that passively diffused across a DOPC lipid bilayer, demonstrating signal transduction across lipid bilayers using steroids. To demonstrate spatial localization of sensing responses, we combined two populations of GUVs containing distinct aptamers and demonstrated target-specific activation in the presence of individual and multiple steroid inputs. Thus, our work introduces a mechanism for using multiple standardized components, which would otherwise cross-react due to sequence complementarity, in a single-tube assay. Protecting DNA-based computing elements from nucleases that are found in living systems is an important problem, and we have shown that our system prevents degradation of isolated DNA components by DNAses. This system was also

DOI: 10.1021/acsami.9b03143
ACS Appl. Mater. Interfaces 2019, 11, 11262−11269

shown to decrease spurious interactions, by preventing fully complementary strands from meeting, and hence interacting with, the A/Q pairs.

A fruitful avenue for future work will be to scale up the complexity of the computation performed within the compartments, in which the aptamer-binding reactions monitored here would be just the first step of a multilayer molecular computing cascade;[6] our group previously demonstrated the use of an aptamer as the input layer of an engineered cascade.[8] Furthermore, developing methods for signaling results back out of a compartment would enable the development of modular computational cascades assembled from reusable, vesicle-isolated subroutines.[30] We note, however, that improved vesicle stability will be necessary for substantially scaled-up cascades of vesicle components. This could be achieved by forming our compartments from polymersomes, which are more stable self-assembled shell structures composed of amphiphilic block copolymers.[31] Another suitable approach could be the use of lipid bilayers on mesoporous silica microparticles to compartmentalize circuits, as demonstrated in our previous work.[32]

MATERIALS AND METHODS

Materials. All oligonucleotides were purchased from Integrated DNA Technologies (IDT, Coralville, IA). Oligonucleotide sequences are presented in Supporting Information Table S1. Unmodified strands were ordered with standard desalting, and the fluorophore-/quencher-tagged strands were purified by high-performance liquid chromatography. Lipids were purchased from Avanti Polar Lipids (Alabaster, AL). Chloroform and hexanes were purchased from OmniSolv (Billerica, MA). PVA, PBS, $MgCl_2$, CS, DC, and DNAse I were purchased from Sigma-Aldrich (St. Louis, MO). Square glass capillaries (OD 1.5 mm, ID 1.05 mm) were purchased from Atlantic International Technology (Rockaway, NJ). Round glass capillaries (OD 1.0 mm, ID 0.58 mm) were purchased from World Precision Instruments (Sarasota, FL). Devcon 5 min epoxy must be used for device fabrication and was purchased from Scientific Commodities Inc. (Lake Havasu City, AZ).

Microfluidics To Generate GUVs. A micropipette puller (P-97, Sutter Instrument, Inc.), at a heat setting of 500, pull strength of 4, velocity of 4, and time setting of 150 for the injection, and collection capillaries were used. For the IA capillary, a heat setting of 600, pull strength of 50, velocity of 50, and time setting of 150 was used. After pulling the capillaries, a microforge (MF-830, Narishige) was used to determine the ID dimensions, which were then adjusted using a 2500 grit sandpaper from Home Depot. All PVA solutions were filtered with 5 μm filters (EMD Millipore) prior to use. Trimethoxy-(octadecyl)silane was distilled (283 °C, under vacuum) prior to use, and devices were remade after each use to ensure efficient silane coats. The oil phase consisted of pure DOPC at 5 mg/mL in a mixture of 36 vol % chloroform and 64 vol % hexane. To form ultrathin GUVs that were stable for up to 5 h, we used a flow rate of 2500 μL/h for both the IA and the oil phases and 10 000 μL/h for the continuous phase.

Fluorimetry. Initial experiments were run to determine the optimal amount of quencher strand required for full quenching and strong ligand-dependent activation (see Supporting Information Figure S1). This was found to be 10 mol % above the aptamer strand concentration. To achieve consistent and maximal quenching, aptamer and quencher strands were incubated at room temperature for 15 min in a PBS solution and then diluted to the desired concentration in 10 wt % PVA in PBS (Supporting Information Figure S2). For the solution-phase experiments, the prehybridized aptamer (50 nM)/quencher (55 nM) complexes were added to 10 wt % PVA solution. Each steroid (150 μM) was added and the solution was incubated at room temperature for 1 h (Figure S3). Each A/Q pair was activated by its ligand (e.g., the DOGS.2 A/Q pair was activated by the DC steroid target), and we saw a minimal increase in fluorescence for the nonspecific steroid (e.g., the DOGS.2 A/Q pair in the presence of CS steroid). This nonspecific activation was minimal compared with the target steroid and was considered a negative response.

The DOGS.2 fluorimetry experiments were performed at room temperature (25 °C) on a Spectramax M2e fluorescent plate reader (Molecular Devices) in a 200 μL reaction volume (FAM: λ_{ex} = 492 nm, λ_{em} = 518 nm). The CSS.1 fluorimetry experiments were performed on a Photon Technology International fluorimeter (ATTO647: λ_{ex} = 647 nm, λ_{em} = 662 nm) because of the excitation wavelengths available on this instrument.

Confocal Fluorescence Microscopy. All confocal experiments were performed on a Zeiss LSM800 confocal microscope at the University of New Mexico Comprehensive Cancer Center. Laser power for the FAM (λ_{ex} = 488 nm, λ_{em} = 520 nm) channel was held constant at 1%, with master gain set to 800 V. Laser power for the ATTO647 (λ_{ex} = 647 nm, λ_{em} = 662 nm) channel was held constant at 4%, with master gain set to 600 V. The pinhole for all experiments was set to 64 μm. A 40× oil emersion objective was used, with a scan speed of 6, and 0.5× magnification for individual GUVs. A 10× objective, with a scan speed of 6, was used when imaging multiple GUVs. A frame size of 2048 × 2048 was used, which corresponds to a pixel size of 0.16 μm with the above settings.

ASSOCIATED CONTENT

Supporting Information

The Supporting Information is available free of charge on the ACS Publications website at DOI: 10.1021/acsami.9b03143.

Optimizing the amount of excess quencher, need for prehybridization, aptamer responses in a homogeneous solution, K_D value for the DC steroid, and raw data for Figure 4 in main text (PDF)

Microfluidic device in operation (MPG)

AUTHOR INFORMATION

Corresponding Authors

*E-mail: graves@unm.edu (S.W.G.).
*E-mail: ncarroll@unm.edu (N.J.C.).
*E-mail: mlakin@cs.unm.edu (M.R.L.).

ORCID

Aurora Fabry-Wood: 0000-0002-0189-0960
Steven W. Graves: 0000-0001-6648-2194
Nick J. Carroll: 0000-0001-7747-7307
Matthew R. Lakin: 0000-0002-8516-4789

Author Contributions

All authors contributed to writing the manuscript. N.J.C. provided microfluidic training and expertise. N.J.C., A.F.-W. and A.O. fabricated the glass capillary microfluidics devices. A.F.-W., M.E.F. and A.O. conducted the fluorimetry experiments. A.F.-W. conducted all confocal experiments. K.-A.Y. and M.N.S. provided aptamer sequences and advice on aptamer use. M.R.L. and A.F.-W. redesigned the CSS.1 aptamer stem sequence. M.N.S., D.S., M.R.L., S.W.G., and N.J.C. supervised the project.

Funding

This material is based on the work supported by the National Science Foundation under grants 1843958, 1525553, 1518861, 1422840, and 1318833. The research reported was also supported by the National Institutes of Health award DA045550.

Notes

The authors declare no competing financial interest.

DOI: 10.1021/acsami.9b03143
ACS Appl. Mater. Interfaces 2019, 11, 11262−11269

■ ACKNOWLEDGMENTS

We kindly thank Andrew P. Shreve for discussion on lipid composition and membrane permeability experiments, Gabriel P. Lopez for his careful reading of this manuscript, and Michael L. Paffett for assistance with confocal microscopy.

■ REFERENCES

(1) Katz, E. *Biomolecular Information Processing: From Logic Systems to Smart Sensors and Actuators*; Wiley-VCH, 2012.
(2) Good, M. C.; Zalatan, J. G.; Lim, W. A. Scaffold Proteins: Hubs for Controlling the Flow of Cellular Information. *Science* **2011**, *332*, 680−686.
(3) Yurke, B.; Turberfield, A. J.; Mills, A. P., Jr; Simmel, F. C.; Neumann, J. L. A DNA-Fuelled Molecular Machine Made of DNA. *Nature* **2000**, *406*, 605−608.
(4) Stojanovic, M. N.; Mitchell, T. E.; Stefanovic, D. Deoxyribozyme-Based Logic Gates. *J. Am. Chem. Soc.* **2002**, *124*, 3555−3561.
(5) Qian, L.; Winfree, E. Scaling Up Digital Circuit Computation with DNA Strand Displacement Cascades. *Science* **2011**, *332*, 1196−1201.
(6) Brown, C. W., III; Lakin, M. R.; Horwitz, E. K.; Fanning, M. L.; West, H. E.; Stefanovic, D.; Graves, S. W. Signal Propagation in Multi-Layer DNAzyme Cascades using Structured Chimeric Substrates. *Angew. Chem., Int. Ed.* **2014**, *53*, 7183−7187.
(7) Seelig, G.; Soloveichik, D.; Zhang, D. Y.; Winfree, E. Enzyme-Free Nucleic Acid Logic Circuits. *Science* **2006**, *314*, 1585−1588.
(8) Brown, C. W., III; Lakin, M. R.; Fabry-Wood, A.; Horwitz, E. K.; Baker, N. A.; Stefanovic, D.; Graves, S. W. A Unified Sensor Architecture for Isothermal Detection of Double-Stranded DNA, Oligonucleotides, and Small Molecules. *ChemBioChem* **2015**, *16*, 725−730.
(9) Jiang, Y. S.; Bhadra, S.; Li, B.; Ellington, A. D. Mismatches Improve the Performance of Strand-Displacement Nucleic Acid Circuits. *Angew. Chem., Int. Ed.* **2014**, *53*, 1845−1848.
(10) Thachuk, C.; Winfree, E.; Soloveichik, D. Leakless DNA Strand Displacement Systems. *DNA Computing and Molecular Programming DNA*; Lecture Notes in Computer Science; Springer, 2015; Vol. *9211*, pp 133−153.
(11) Teichmann, M.; Kopperger, E.; Simmel, F. C. Robustness of Localized DNA Strand Displacement Cascades. *ACS Nano* **2014**, *8*, 8487−8496.
(12) Ruiz, I. M.; Arbona, J.-M.; Lad, A.; Mendoza, O.; Aimé, J.-P.; Elezgaray, J. Connecting localized DNA strand displacement reactions. *Nanoscale* **2015**, *7*, 12970−12978.
(13) Chatterjee, G.; Dalchau, N.; Muscat, R. A.; Phillips, A.; Seelig, G. A Spatially Localized Architecture for Fast and Modular DNA Computing. *Nat. Nanotechnol.* **2017**, *12*, 920−927.
(14) Thubagere, A. J.; Li, W.; Johnson, R. F.; Chen, Z.; Doroudi, S.; Lee, Y. L.; Izatt, G.; Wittman, S.; Srinivas, N.; Woods, D.; Winfree, E.; Qian, L. A Cargo-Sorting DNA Robot. *Science* **2017**, *357*, No. eaan6558.
(15) Bui, H.; Shah, S.; Mokhtar, R.; Song, T.; Garg, S.; Reif, J. Localized DNA Hybridization Chain Reactions on DNA Origami. *ACS Nano* **2018**, *12*, 1146−1155.
(16) Yang, N. J.; Hinner, M. J. Getting Across the Cell Membrane: An Overview for Small Molecules, Peptides, and Proteins. *Site-Specific Protein Labeling*; Methods in Molecular Biology; Springer New York: New York, NY, 2014; Vol. *1266*, pp 29−53.
(17) Arriaga, L. R.; Datta, S. S.; Kim, S.-H.; Amstad, E.; Kodger, T. E.; Monroy, F.; Weitz, D. A. Ultrathin Shell Double Emulsion Templated Giant Unilamellar Lipid Vesicles with Controlled Microdomain Formation. *Small* **2014**, *10*, 950−956.
(18) Yang, K.-A.; Chun, H.; Zhang, Y.; Pecic, S.; Nakatsuka, N.; Andrews, A. M.; Worgall, T. S.; Stojanovic, M. N. High-Affinity Nucleic-Acid-Based Receptors for Steroids. *ACS Chem. Biol.* **2017**, *12*, 3103−3112.
(19) Groves, B.; Chen, Y.-J.; Zurla, C.; Pochekailov, S.; Kirschman, J. L.; Santangelo, P. J.; Seelig, G. Computing in Mammalian Cells with Nucleic Acid Strand Exchange. *Nat. Nanotechnol.* **2016**, *11*, 287−294.
(20) Mei, Q.; Wei, X.; Su, F.; Liu, Y.; Youngbull, C.; Johnson, R.; Lindsay, S.; Yan, H.; Meldrum, D. Stability of DNA Origami Nanoarrays in Cell Lysate. *Nano Lett.* **2011**, *11*, 1477−1482.
(21) Chen, Y.-J.; Groves, B.; Muscat, R. A.; Seelig, G. DNA Nanotechnology from the Test Tube to the Cell. *Nat. Nanotechnol.* **2015**, *10*, 748−760.
(22) Jiang, D.; Sun, Y.; Li, J.; Li, Q.; Lv, M.; Zhu, B.; Tian, T.; Cheng, D.; Xia, J.; Zhang, L.; Wang, L.; Huang, Q.; Shi, J.; Fan, C. Multiple-Armed Tetrahedral DNA Nanostructures for Tumor-Targeting, Dual-Modality in Vivo Imaging. *ACS Appl. Mater. Interfaces* **2016**, *8*, 4378−4384.
(23) Kim, S.-H.; Kim, J. W.; Cho, J.-C.; Weitz, D. A. Double-Emulsion Drops with Ultra-Thin Shells for Capsule Templates. *Lab Chip* **2011**, *11*, 3162−3166.
(24) Yalkowsky, S. H.; He, Y.; Jain, P. *Handbook of Aqueous Solubility Data*, 2nd ed.; CRC Press, 2010.
(25) Yasuga, H.; Kawano, R.; Takinoue, M.; Tsuji, Y.; Osaki, T.; Kamiya, K.; Miki, N.; Takeuchi, S. Droplet Network Connected by Biological Nanopores for DNA Computing. In *Transducers and Eurosensors XXVII: The 17th International Conference on Solid-State Sensors, Actuators and Microsystems, TRANSDUCERS and EUROSENSORS*, 2013; pp 1221−1222.
(26) Yasuga, H.; Kawano, R.; Takinoue, M.; Tsuji, Y.; Osaki, T.; Kamiya, K.; Miki, N.; Takeuchi, S. Logic Gate Operation by DNA Translocation through Biological Nanopores. *PLoS One* **2016**, *11*, No. e0149667.
(27) Langecker, M.; Arnaut, V.; List, J.; Simmel, F. C. DNA Nanostructures Interacting with Lipid Bilayer Membranes. *Acc. Chem. Res.* **2014**, *47*, 1807−1815.
(28) Howorka, S. Building Membrane Nanopores. *Nat. Nanotechnol.* **2017**, *12*, 619−630.
(29) Padirac, A.; Fujii, T.; Rondelez, Y. Quencher-free multiplexed monitoring of DNA reaction circuits. *Nucleic Acids Res.* **2012**, *40*, No. e118.
(30) Gines, G.; Zadorin, A. S.; Galas, J.-C.; Fujii, T.; Estevez-Torres, A.; Rondelez, Y. Microscopic agents programmed by DNA circuits. *Nat. Nanotechnol.* **2017**, *12*, 351−359.
(31) Discher, D. E.; Ahmed, F. Polymersomes. *Annu. Rev. Biomed. Eng.* **2006**, *8*, 323−341.
(32) Fabry-Wood, A.; Fetrow, M. E.; Brown, C. W., III; Baker, N. A.; Fernandez Oropeza, N.; Shreve, A. P.; Montaño, G. A.; Stefanovic, D.; Lakin, M. R.; Graves, S. W. A Microsphere-Supported Lipid Bilayer Platform for DNA Reactions on a Fluid Surface. *ACS Appl. Mater. Interfaces* **2017**, *9*, 30185−30195.

DOI: 10.1021/acsami.9b03143
ACS Appl. Mater. Interfaces 2019, 11, 11262−11269